Polyethylene Catalytic Hydrocracking by PtHZSM-5, PtHY, and PtHMCM-41

Nathan D. Hesse, Robert L. White

Department of Chemistry and Biochemistry, University of Oklahoma, Norman, Oklahoma 73019

Received 23 April 2003; accepted 23 October 2003

ABSTRACT: The mechanisms involved in polyethylene catalytic hydrocracking are investigated by monitoring temperature-dependent evolution profiles derived from mass spectra obtained while polymer/catalyst samples were heated at a constant rate. Repetitive injection gas chromatography/mass spectrometry (GC/MS) results are used to identify class-specific fragment ions that represent paraffins, olefins, and alkyl aromatics. Class-specific ion signals are used to generate isoconversion-effective activation energy plots from which mechanistic comparisons are made. Studies using PtHZSM-5, PtHY, and PtHMCM-41 bifunctional solid acid catalysts in helium and hydrogen are reported. The effects of hydrogen on polyethylene cracking are dramatic and result in significant changes to isoconversion-effective activation energies. Catalytic cracking mechanisms for the three catalysts are compared and differences are explained by a combination of pore size and acidity effects.
 J Appl Polym Sci 92: 1293–1301, 2004

Key words: polyethylene; catalysis; thermal properties; activation energy

INTRODUCTION

Disposal of municipal solid waste (MSW) poses a never-ending environmental challenge. The amount of MSW generated in the United States increased from 88.1 million tons in 1960 to 231.9 million tons in 2000.[1] Waste plastics are the most rapidly growing MSW component. The rate of plastic waste generation increased 10-fold between 1960 and 2000.[2] Between 1991 and 2000, plastic commodity manufacturing grew by 6.5% annually, compared to 1.8% for overall manufacturing.[3] Plastics were responsible for 10.7% of MSW weight and about 20% of MSW volume in 2000.[1] Currently, MSW plastics are recycled at a rate of only 5.4%.[2] One reason for this relatively low recycling rate is the need to sort plastics by polymer type prior to most recycling processes. There are few recycling options for unsorted plastic waste, multilayer plastics, and plastic composites. In addition to conventional recycling options, pyrolysis and catalytic cracking can be used to remove waste plastics from MSW by converting them to hydrocarbon mixtures. Unlike other recycling options, pyrolysis and catalytic cracking do not require polymer type sorting. Catalytic cracking is preferred over pyrolysis because it typically produces smaller hydrocarbons, yielding higher value liquid and gaseous products.

Correspondence to: R. L. White (rlwhite@ou.edu).

Journal of Applied Polymer Science, Vol. 92, 1293–1301 (2004)

Previous polymer cracking studies have focused primarily on polyethylene (PE) because it is the most abundant polymer in MSW. Most studies have involved the use of solid-state acid catalysts. For example, Ochoa and coworkers employed a series of silica–alumina catalysts with varying Brönsted/Lewis acid site ratios and determined that the oil yield from medium-density polyethylene was dictated by the catalyst Brönsted acidity.[4] Aguado et al. compared the activities and product selectivities of PE cracking by using HZSM-5 and MCM-41 catalysts.[5,6] They found that HZSM-5 was more active for PE cracking, but selectivity for gasoline and middle distillates (C_5–C_{12}) was higher for MCM-41. Sakata and coworkers produced fuel oil from PE by using silica–alumina, ZSM-5, and nonacidic mesoporous silica.[7,8] Sharratt and coworkers used a fluidized-bed reactor and HZSM-5 catalyst to crack PE with 90 wt % yield at 360°C[9] and then extended their studies to include silica–alumina, mordenite, and HY.[10]

The yield of unsaturated catalytic cracking products can be reduced by the addition of hydrogen to cracking atmospheres. Dufaud and Basset demonstrated this by employing a zirconium hydride Ziegler–Natta catalyst to crack PE in a hydrogen atmosphere.[11] Ding et al. studied the hydroconversion of PE with sulfided Ni and NiMo silica–alumina and compared these catalysts to HZSM-5.[12] They found that Ni/silica–alumina produced higher quality liquid products (i.e., more isoparaffins and fewer aromatics). Walendziewski et al. studied PE hydrocracking in autoclaves and reported that the addition of catalysts decreased

the boiling range and unsaturation of liquid products compared to thermal and catalytic cracking.[13,14]

Although most previous reports focus on correlating variations in product slate with catalyst properties, some studies have attempted to compare catalyst activation energies obtained by using thermal analysis techniques. Garforth et al. used activation energies derived from thermogravimetry (TG) measurements to compare the cracking properties of ZSM-5, HY, and MCM-41.[15] They found that coking was most significant for HY and that MCM-41 exhibited the lowest cracking activation energy. In a similar study, Fernandes et al. compared the TG-derived activation energy for PE thermal decomposition with that for HZSM-5 catalytic cracking and found that the catalyst reduced the activation energy by more than a factor of 2.[16,17] Lin and coworkers characterized the deactivation of USY zeolite by monitoring changes in the TG properties of polymer/catalyst mixtures.[18]

A detailed study of PE hydrocracking by PtHZSM-5, PtHY, and PtHMCM-41 bifunctional aluminosilicate catalysts is presented here. Volatile product slates and class-specific evolution profiles derived from repetitive injection GC/MS[19,20] analysis of purge gas streams reveal the order in which volatile products are produced when the cracking temperature is linearly increased. Catalyst activity evaluations are made based on comparisons of class-specific effective activation energy profiles derived from mass spectrometric analyses.[21]

EXPERIMENTAL

Materials

Polyethylene with a reported average molecular weight of 700 g/mol and melting temperature range of 80–90°C was purchased from Polysciences Inc. (Warrington, PA). The hydrogen form of ZSM-5 (Mobil Five (MFI) crystal structure, 5.3 × 5.6 and 5.1 × 5.5 Å intersecting channels) was obtained from Mobil Oil Corp. (Paulsboro, NJ). The framework of the HZSM-5 catalyst was reported to contain 1.5 wt % alumina. NaY-54 FAU zeolite with a 7.4 Å channel diameter and 12.3 Å channel intersections was obtained from Universal Oil Products (Danbury, CT). The silica–alumina ratio for this catalyst was reported to be 5.30. Sodium ions were removed from this catalyst by ion exchange with 1.0*M* ammonium nitrate solution. About 1.0 g of catalyst was placed in 250 mL NH_4NO_3 and the mixture was refluxed with constant stirring overnight. The NH_4Y was dried at 110°C and then calcined at 550°C for 3 h to produce HY. The mesoporous MCM-41 catalyst, with a honeycomb-like structure with parallel pores (15–150 Å pore size range), was synthesized in our laboratory by using procedures described in the literature.[22–24] Dodecyltrimethyl ammonium bromide (DTMABr) and tetramethyl ammonium hydroxide pentahydrate (TMAH) were used as template molecules. A solution containing 11.47 g LUDOX® (30 wt % SiO_2) and 10.0 g TMAH in 16.4 mL of distilled water was prepared and then allowed to age for 2 days. Then, 20.0 g DTMABr and 0.296 g Al_2O_3 were added to the aged solution with thorough mixing. A second solution was prepared by dissolving 1.29 g of NaOH in 5.46 mL of distilled water and then 2.5 g of SiO_2 was added. The two solutions were combined and the resulting mixture was autoclaved at 140°C for 4 days. The resulting solid was filtered, rinsed with distilled water, and dried at 110°C. The dried powder was calcined at 600°C for 4 h to remove the organic templates from the silica–alumina framework. The resulting NaMCM-41 was ion-exchanged as described previously to remove sodium ions and then dried and calcined for 6 h at 540°C to obtain HMCM-41. Electron microprobe analysis revealed that the Al_2O_3 content of this catalyst was about 17 wt %.

Bifunctional catalysts were prepared by adding approximately 1 wt % platinum to the solid acid catalysts by an incipient wetness method described by Jacobs et al.[25] Hydrogen hexachloroplatinate (IV) hydrate ($H_2PtCl_6 \cdot xH_2O$) of 99.9% purity and 38–40 wt % platinum was obtained from Aldrich Chemical Co. (Milwaukee, WI). The platinum solution was made by adding 0.0418 g H_2PtCl_6 to 1.0 mL of distilled water. About 100 mg of catalyst was mixed with 0.63 mL of the platinum solution and the slurry was then stirred with a Buchner Instruments (Kansas City, MO) VV mini-roto-evaporation apparatus at ambient conditions for several hours. The slurry was dried at 110°C for 2 h followed by calcination at 400°C for 2 h. Each bifunctional catalyst was heated in hydrogen (25 mL/min) for 2 h at 500°C to reduce the platinum.

Catalyst and polymer powders were combined to prepare samples. Small particles were used to maximize contact between the polymer and catalysts. The PtHY particle sizes used for preparing samples were less than 180 μm, whereas PtHZSM-5 and PtHMCM-41 particles were less than 250 μm. The PE powder used for sample preparation consisted of particles that were less than 150 μm. Polymer/catalyst samples were prepared by mechanically mixing ~ 10% by weight PE with catalyst.

Repetitive injection GC/MS conditions

The apparatus and procedures for acquiring repetitive injection gas chromatography/mass spectrometry (GC/MS) mass spectra are described in detail elsewhere.[20] The same heating and mass spectrometer conditions were used for all PE/catalyst samples in this study. PE/catalyst samples weighing approximately 15 mg were heated in a tube furnace at 2°C/

min from 100 to 400°C. For sample analyses in an inert atmosphere, the tube furnace was purged with helium (25 mL/min) for 30 min prior to heating. For analyses in a hydrogen atmosphere, the helium purge was followed by a 30-min hydrogen purge (25 mL/min) prior to sample heating. Total ion current (TIC) chromatograms were obtained by injecting purge gas into the GC at 5-min (10°C) intervals beginning at 120°C for PE/PtHZSM-5 samples and 180°C for PE/PtHY and PE/PtHMCM-41 samples. After injection, the GC oven temperature was held at −50°C for 0.3 min followed by a ramp to 80°C at 50°C/min and a second ramp to 200°C at 109°C/min. After the final temperature was reached, the GC oven was made ready for another injection within 45 s by cooling with liquid N_2 to −50°C. A 10-m, 0.25-mm inner diameter DB-1 capillary GC column with a 0.25-μm stationary phase thickness and a 2-mL/min helium carrier gas flow rate were employed for separations. The quadruple mass spectrometer was set to scan from *m/z* 15 to 160 at a rate of 3.425 scans/s. Chromatographic eluants were identified by library searching with a 38,000 spectrum library.

Isoconversion effective activation energy measurements

The apparatus and procedures for computing class-specific isoconversion-effective activation energies from mass spectrometric information are described in detail elsewhere.[21] Approximately 5 mg PE/catalyst samples were heated in 50 mL/min helium or hydrogen. The mass spectrometer was set to scan from *m/z* 35 to 95. Separate samples were subjected to linear heating ramps of 5, 10, 15, and 25°C/min under the same reaction conditions. Mass spectrometer data collection was initiated when the sample temperature reached 100°C for PE/PtHZSM-5 samples and 120°C for PE/PtHY and PE/PtHMCM-41 samples. Isoconversion effective activation energies were computed at 1% conversion increments.

RESULTS

Repetitive injection GC/MS analyses of evolved gases generated when PE/catalyst samples were heated resulted in a series of gas chromatograms. Each chromatogram was representative of the volatile product distribution at the instant that the purge gas was injected into the GC. Chromatograms typically contained more than 30 peaks, most of which were baseline resolved. Species-specific evolution temperature profiles were generated by plotting the chromatographic peak areas for selected products as a function of the sample temperature at which the injection was made.[19] Class-specific evolution profiles shown here were made from species-specific profiles by summing peak areas for volatile products of the same type (i.e., paraffins, olefins, or alkyl aromatics) that had the same number of carbon atoms.

Repetitive injection chromatogram mass spectra were employed to identify class-specific fragment ions for use in effective activation energy calculations and to compute selectivities for these ions. By comparing selected ion profiles with total ion current chromatograms, it was determined that *m/z* 57, 55, and 91 could be used to represent paraffins, olefins, and alkyl aromatics, respectively. Virtually all of the *m/z* 91 ion signal could be attributed to alkyl aromatics. Unfortunately, the *m/z* 57 and 55 ion signals could not always be attributed solely to paraffins and olefins, respectively. To determine the selectivity of these ions for their respective product classes, a selectivity value was calculated by computing the ratio of the ion signal contribution from the desired class to the total ion signal for the target *m/z* value. This calculation was repeated for each repetitive injection chromatogram to obtain selectivity profiles as a function of sample temperature.

PtHZSM-5

Figure 1 shows the class-specific evolution profiles for (a) paraffin, (b) olefin, and (c) alkyl aromatic volatile products for the PE/PtHZSM-5 sample heated in helium. C_3–C_{10} hydrocarbons were detected and C_3–C_6 hydrocarbons dominated the volatile products. Below 200°C, volatile mixtures were composed mostly of C_4–C_7 paraffins. As the sample temperature increased, C_4 olefins became the most abundant volatile products. The temperature corresponding to the maximum paraffin and olefin evolution rates was 240°C. Alkyl aromatic volatile products were detected initially at 240°C and their evolution maximized at 280–290°C. C_2-substituted phenyl isomers were the most abundant volatile alkyl aromatic species. Figure 2 shows the class-specific evolution profiles for (a) paraffin, (b) olefin, and (c) alkyl aromatic volatile products for the PE/PtHZSM-5 sample heated in hydrogen. As expected, paraffins dominated the hydrocracking volatile product slate and olefin and alkyl aromatic yields were greatly reduced compared to results obtained when the same sample was heated in helium. Similar to Figure 1(a), the paraffin profile for the PE/PtHZSM-5 sample heated in hydrogen exhibited two maxima. Below 200°C, volatile product mixtures were composed entirely of paraffins. As the sample temperature increased, a wide range of C_3–C_{10} volatile paraffins were formed, with C_5 and C_6 paraffins being the most abundant volatile products detected. The paraffin evolution profile in hydrogen extended to a higher temperature than when the sample was heated in helium. In contrast to the PE/PtHZSM-5 sample heated in helium, C_3 and C_4 olefins were not detected

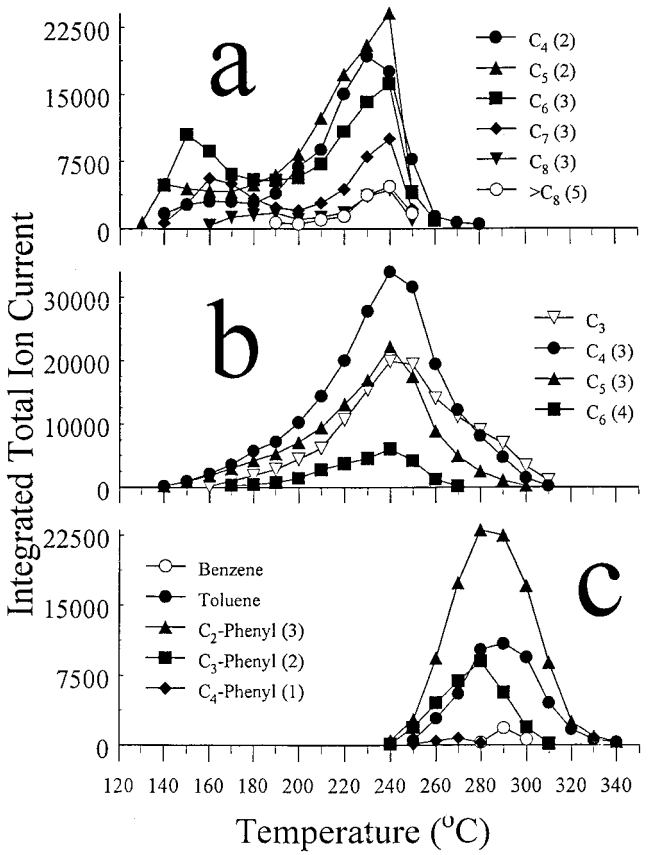

Figure 1 Evolution profiles for (a) paraffins, (b) olefins, and (c) alkyl aromatics for the PE/PtHZSM-5 sample heated in helium.

and olefins larger than C_6 were detected in significant yield.

Figure 3(a) shows class-specific effective activation energy (E_a) versus temperature plots generated for the evolution of paraffins (*m/z* 57), olefins (*m/z* 55), and alkyl aromatics (*m/z* 91) when the PE/PtHZSM-5 sample was heated in helium. The selectivity of *m/z* 57 for paraffins was about 90% between 140 and 240°C. Paraffin evolution E_a values above 240°C were not included in Figure 3(a) because the *m/z* 57 selectivity for paraffins decreased dramatically above this temperature due to increased contributions to the *m/z* 57 ion signal from olefins. The selectivities of *m/z* 55 for olefins and *m/z* 91 for alkyl aromatics were at least 99% for the values plotted in Figure 3(a). Olefin E_a values below 250°C were not included in Figure 3(a) because the *m/z* 55 selectivity for olefins was significantly reduced due to contributions to the *m/z* 55 ion signal from paraffins. The paraffin E_a plot has two distinct regions. The initial E_a value for paraffin formation was about 24 kcal/mol and remained relatively constant until 180°C. Isoconversion E_a values increased to approximately 36 kcal/mol by 240°C. The olefin E_a value was about 35 kcal/mol at 250°C and gradually decreased to about 31 kcal/mol at 300°C. The alkyl aromatic E_a value was relatively constant at about 34 kcal/mol from 280 to 330°C.

Figure 3(b) shows the paraffin-specific effective E_a versus temperature plot for the PE/PtHZSM-5 sample heated in hydrogen. The *m/z* 57 ion signal selectivity for paraffins was 99%. Similar to Figure 3(a), the paraffin E_a plot exhibits an increase from 24 to about 40 kcal/mol. Above 220°C, E_a values gradually decreased to about 30 kcal/mol at 310°C. Smaller error bars in Figure 3(b) compared to Figure 3(a) reflect the fact that paraffins were by far the dominant volatile product when the PE/PtHZSM-5 sample was heated in hydrogen. As a result, the *m/z* 57 ion signals were larger than those detected in helium and the *m/z* 57 selectivity for paraffins was much greater (at least 99%) when the sample was heated in hydrogen.

PtHY

Figure 4 shows the class-specific evolution profiles calculated for (a) paraffin, (b) olefin, and (c) alkyl aromatic volatile products for the PE/PtHY sample heated in helium. C_3–C_{10} hydrocarbons were detected and C_6–C_{10} paraffins were the dominant volatile species. The temperature corresponding to the maximum

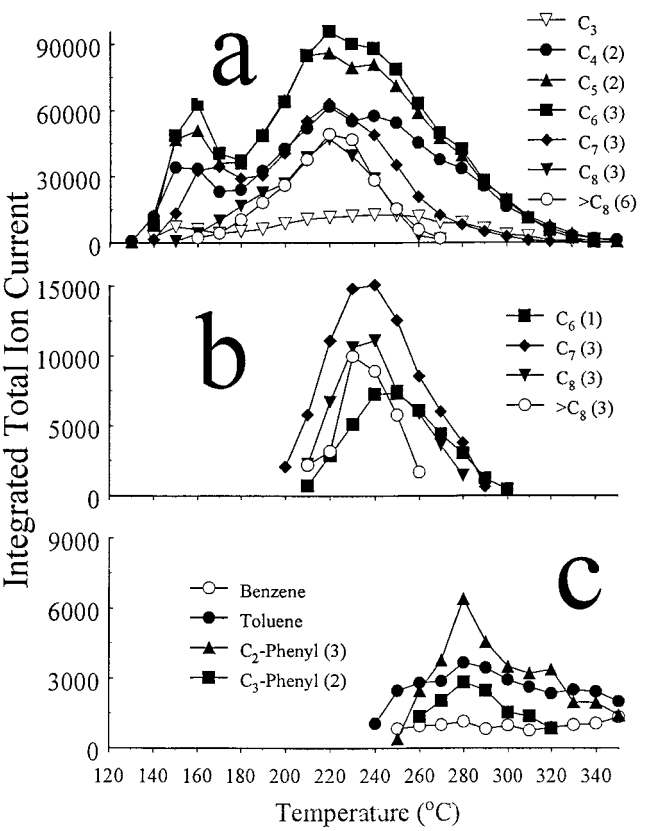

Figure 2 Evolution profiles for (a) paraffins, (b) olefins, and (c) alkyl aromatics for the PE/PtHZSM-5 sample heated in hydrogen.

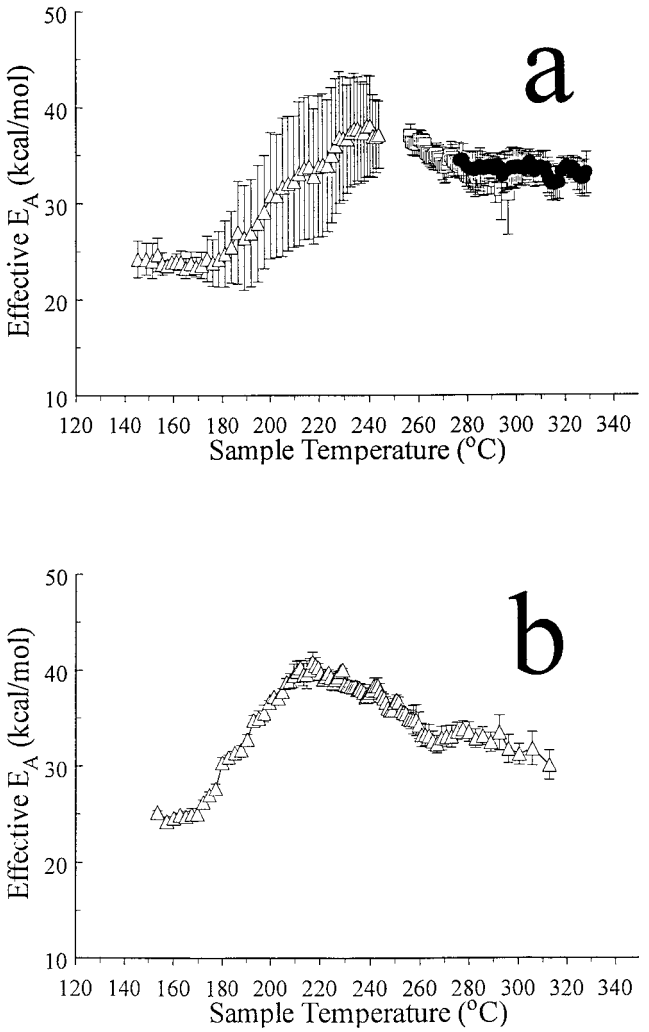

Figure 3 PE/PtHZSM-5 effective activation energy profiles for (a) paraffins (△), olefins (□), and alkyl aromatics (●) in helium; (b) paraffins (△) in hydrogen.

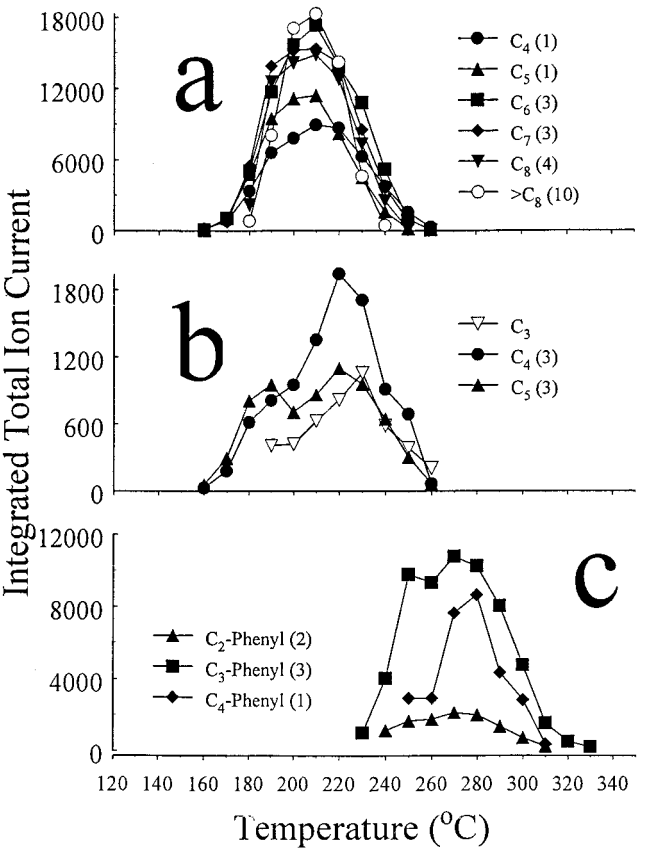

Figure 4 Evolution profiles for (a) paraffins, (b) olefins, and (c) alkyl aromatics for the PE/PtHY sample heated in helium.

paraffin evolution rate was 210°C. No volatile paraffin or olefin products were detected above 260°C. Alkyl aromatic volatile products were initially detected at 230°C and their evolution maximized at 270–280°C. The fraction of alkyl aromatics detected was similar to that for the PE/PtHZSM-5 sample heated in helium.

Figure 5 shows the class-specific evolution profiles for (a) paraffin and (b) olefin volatile products for the PE/PtHY sample heated in hydrogen. Seventeen different paraffins with at least nine carbon atoms dominated the volatile products. The temperature corresponding to the maximum paraffin evolution rate was 260°C. Compared to the same sample heated in helium, paraffin and olefin evolution profiles were narrower and shifted to a slightly higher temperature. Volatile alkyl aromatic yields were insignificant compared to the paraffin and olefin yields.

Figure 6(a) shows the E_a versus temperature profiles for paraffin and alkyl aromatic evolutions when the sample was heated in helium. The *m/z* 57 and *m/z* 91 ion signal selectivities for paraffins and alkyl aromatics were at least 99%. The initial E_a value for paraffin formation

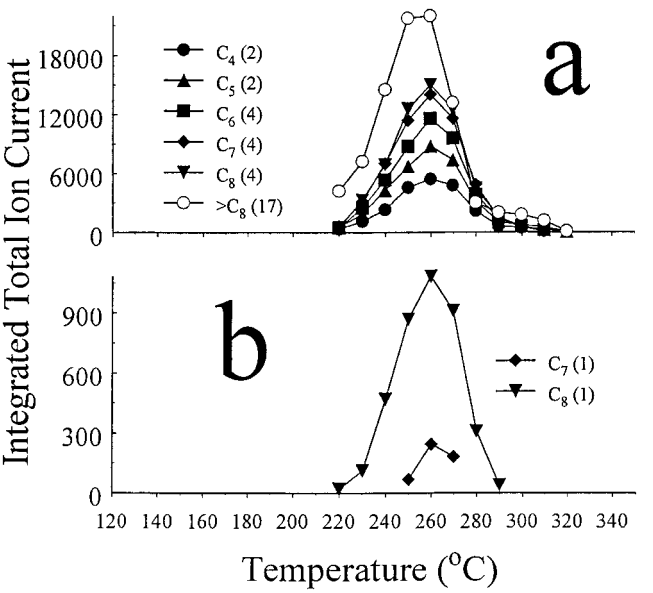

Figure 5 Evolution profiles for (a) paraffins and (b) olefins for the PE/PtHY sample heated in hydrogen.

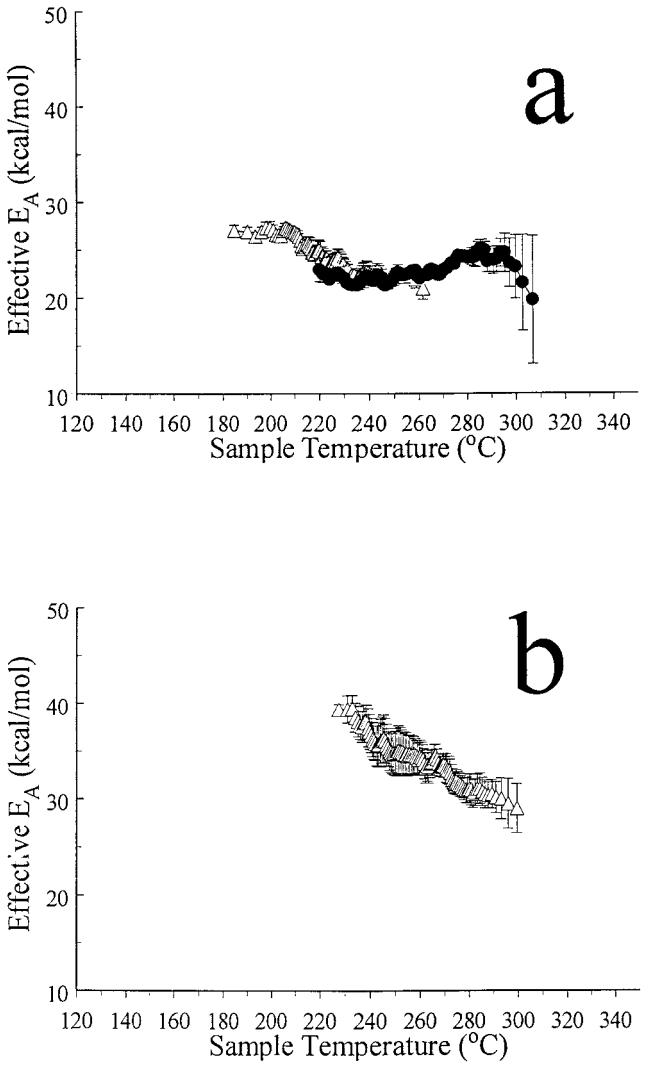

Figure 6 PE/PtHY effective activation energy profiles for (a) paraffins (△) and alkyl aromatics (●) in helium; (b) paraffins (△) in hydrogen.

was about 27 kcal/mol at 180°C and decreased to approximately 23 kcal/mol by 260°C. The initial E_a value for alkyl aromatic formation was about 23 kcal/mol at 220°C and remained relatively constant until 310°C. The alkyl aromatic E_a value calculated for the PE/PtHY sample heated in helium was 10 kcal/mol lower than that for the PE/PtHZSM-5 sample. Figure 6(b) shows the paraffin E_a versus temperature profile for the PE/PtHY sample heated in hydrogen. The *m/z* 57 ion signal selectivity for paraffins was at least 99%. The E_a value for paraffin formation was 38 kcal/mol at 230°C and decreased to 28 kcal/mol by 300°C. The initial paraffin E_a value for the PE/PtHY sample heated in hydrogen was 10 kcal/mol higher than the E_a value for the same sample heated in helium.

PtHMCM-41

Figure 7 shows class-specific evolution profiles for (a) paraffin and (b) olefin volatile products when the PE/PtHMCM-41 sample was heated in helium. The shapes of the paraffin and olefin volatile product evolution profiles were similar. C_3–C_{10} hydrocarbons were detected and C_4–C_{10} olefins were the dominant volatile species. The temperature corresponding to the maximum olefin evolution rate was 250°C. Figure 8 shows the class-specific evolution profile for paraffin volatile products for the PE/PtHMCM-41 sample heated in hydrogen. Volatile paraffins with more than eight carbon atoms dominated the product slate. The paraffin evolution profile was narrower and shifted to a higher temperature compared to results obtained when the same sample was heated in helium. Volatile alkyl aromatic products were not detected for the PE/PtHMCM-41 sample heated in either helium or hydrogen.

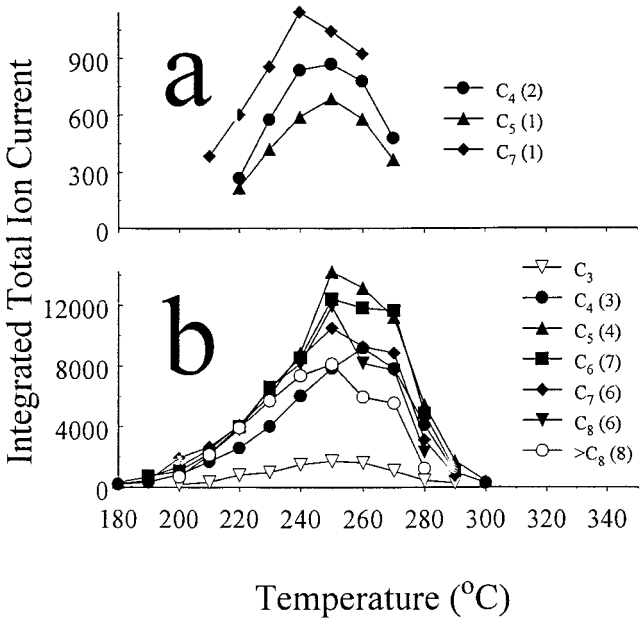

Figure 7 Evolution profiles for (a) paraffins and (b) olefins for the PE/PtHMCM-41 sample heated in helium.

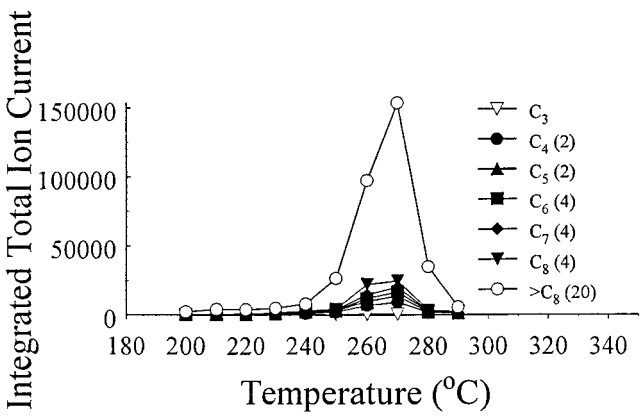

Figure 8 Paraffin evolution profiles for the PE/PtHMCM-41 sample heated in hydrogen.

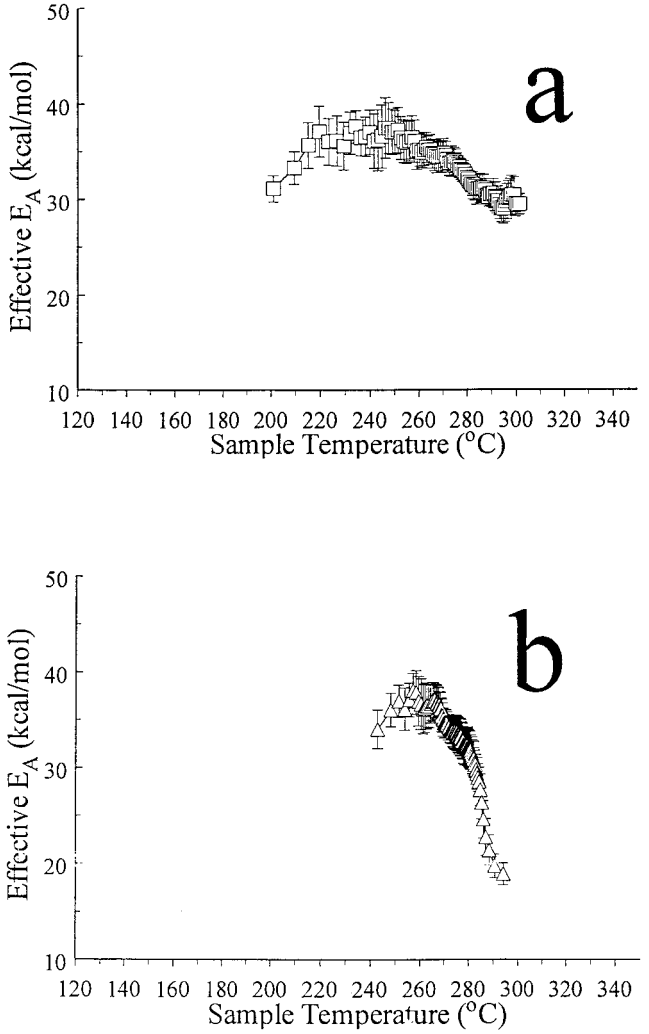

Figure 9 PE/PtHMCM-41 effective activation energy profiles for (a) olefins (□) in helium; (b) paraffins (△) in hydrogen.

Figure 9(a) shows the olefin evolution E_a versus temperature plot for the PE/PtHMCM-41 sample heated in helium. The *m/z* 55 ion signal selectivity for olefins was at least 99%. The E_a value for olefin formation was 32 kcal/mol at 200°C, increased to about 37°C by 240°C, and then decreased to 30 kcal/mol by 300°C. Figure 9(b) shows the paraffin E_a versus temperature plot for the PE/PtHMCM-41 sample heated in hydrogen. The *m/z* 57 ion signal selectivity for paraffins was at least 99% for the data plotted. The paraffin evolution E_a value was 32 kcal/mol at 240°C, increased to 36°C by 260°C, and decreased to 18 kcal/mol by 300°C.

DISCUSSION

The hydrocracking effect on polyethylene decomposition is clearly evident in the makeup of the volatile product slates for the three bifunctional catalysts. As expected, olefin and alkyl aromatic yields diminished and paraffin yields increased substantially when hydrogen was added to the cracking atmosphere. The most dramatic change to the paraffin–olefin ratio was found for the PtHMCM-41 catalyst (Table I). As shown in Table I, the presence of hydrogen also significantly reduced the quantity of residue remaining after catalytic cracking. These effects are well-known consequences of hydrocracking with bifunctional catalysts containing platinum.[26–28]

Paraffin evolution profiles for the PtHZSM-5 catalyst in helium and hydrogen exhibited bimodal features. Volatile paraffins were initially detected at 130°C. In both helium and hydrogen, paraffin evolution maximized between 150 and 160°C. A drop in paraffin abundance and a second maximum at a higher temperature followed the initial evolution maximum. The presence of two maxima in paraffin evolution profiles suggests that there were two polyethylene cracking pathways leading to volatile paraffins and that these pathways were available in helium and hydrogen.

The polyethylene melting point was determined to be about 90°C. Thus, PtHZSM-5 cracking products detected at 130°C were derived from the polymer melt. The average molecular weight of the polyethylene employed for these studies was 700, which means that the average polymer chain contained about 50 carbon atoms. These long polymer chains would have difficulty accessing the small pores of HZSM-5. Thus, initial cracking products more likely resulted from reactions outside of the catalyst pores. Reaction mechanisms involving initial polymer catalytic cracking on the outside of zeolite pores have been proposed previously.[29,30] If the first evolution maximum is associated with cracking outside of catalyst pores, the second maximum might be due to additional cracking that occurred when the zeolite pores became accessible to polymer melt. Above 180°C, short polymer segments could more easily enter zeolite channels. In contrast to the paraffin profiles, the evolution profiles for olefins in helium and hydrogen exhibit only a single maximum with much lower yields at low tem-

TABLE I
Paraffin–Olefin Ratio and Residue

	P/O ratio[a]		Residue (%)[b]	
Catalyst	He	H_2	He	H_2
PtHZSM-5	0.86	18	3	<1
PtHY	19	98	26	9
PtHMCM-41	0.03	98	16	5

[a] Computed by dividing the sum of the TIC chromatographic peak areas for paraffins by the corresponding sum for olefin volatile products.

[b] Defined as the percentage of initial polymer mass remaining after catalytic cracking.

perature. Evidently, low-temperature carbocation disproportionation reactions, which yield paraffins, occur more readily than β-scission reactions, which are thought to be responsible for most olefin products.[31]

The PtHZSM-5 paraffin evolution profile in hydrogen was significantly broader than the corresponding helium profile. In addition, C_3 paraffins were detected in hydrogen but not in helium. C_3 paraffins likely resulted from hydrogenation of propene, which was detected in helium but not in hydrogen. In fact, the hydrocracking paraffin yield above 270°C was likely due to hydrogenation of initially formed C_3–C_7 olefins, which were detected in helium in much greater yields. The substantial reduction in alkyl aromatic yields in hydrogen compared to helium is evidence that formation of conjugated unsaturation in the polymer melt was hindered by the hydrogenation activity of the bifunctional catalyst.

Paraffin effective activation energy plots for the PtHZSM-5 catalyst (Fig. 3) reflect the bimodal nature of the evolution profiles. In both helium and hydrogen, initial values were near 25 kcal/mol. Above 180°C, effective activation energies gradually increased to about 40 kcal/mol. This increase in activation energy may be due to increased steric hindrance for cracking reactions that take place within HZSM-5 channels.

Unlike PtHZSM-5, the PtHY volatile product evolution profiles and effective activation energy plots do not exhibit bimodal features. Volatile paraffins and olefins were first detected at 160°C, which was higher than the temperature at which volatiles were first detected for PtHZSM-5. This suggests that PtHZSM-5 sites at which polymer cracking started could better facilitate carbocation disproportionation reactions than those accessible in PtHY. These sites are most likely located outside of zeolite channels, where there is sufficient space for bimolecular disproportionation reactions. Unlike PtHZSM-5, PtHY volatile paraffin yields in helium were substantially greater than olefin yields. Although propene was detected in helium, propane was not detected in hydrogen. The relative propene, butene, and pentene yields for PtHY in helium were much lower than for PtHZSM-5. Consequently, contributions to the paraffin volatile product slate in hydrogen attributed to olefin hydrogenation were much less than for PtHZSM-5. Only C_7 and C_8 olefins were detected and no alkyl aromatics were detected for the PtHY catalyst in hydrogen. The lack of alkyl aromatics and appearance of larger olefin molecules in hydrogen compared to helium is consistent with the substantial decrease in residue when hydrogen was present (Table I) and reflects the impact of hydrogenation on polymer cracking reactions.

The temperature range for alkyl aromatics evolution for the PtHY catalyst in helium was similar to that for the PtHZSM-5 catalyst. However, the effective activation energy for alkyl aromatics evolution was about 10 kcal/mol lower for PtHY compared to PtHZSM-5. The higher activation energy for PtHZSM-5 may have been due to the smaller channels of HZSM-5 compared to HY. Although the HZSM-5 channels may facilitate conjugated bond cyclization reactions, the smaller HZSM-5 channels also hinder the release of aromatic products from the catalyst. The larger zeolite channel diameter of HY is also likely responsible for the fact that the most abundant PtHY alkyl products in helium were C_3-phenyl species, whereas C_2-phenyl products dominated the PtHZSM-5 product slate. The PtHY volatile paraffin and olefin evolution profiles in hydrogen are narrower and shifted to a higher temperature by about 50°C compared to the profiles obtained in helium. This is consistent with the higher paraffin evolution effective activation energies in hydrogen compared to helium (Fig. 6). Increased effective activation energies for catalytic hydrocracking compared to catalytic cracking have been reported previously.[32,33]

The primary volatile products of polyethylene cracking in helium by the PtHMCM-41 catalyst were olefins (Fig. 7). Unlike the other catalysts, alkyl aromatics were not detected for the PtHMCM-41 catalyst. HMCM-41 pores are much larger than HZSM-5 and HY pores. Ammonia TPD measurements of the three catalysts revealed that the HMCM-41 catalyst also had the weakest acid sites.[19] Strong acid sites facilitate disproportion reactions that form paraffins and small pores are required for aromatization reactions. These processes were of minor importance for the PtHMCM-41 catalyst. The effect of hydrogenation on the catalytic cracking ability of PtHMCM-41 was dramatic. Volatile paraffins were the sole products detected in hydrogen and only 5% of the initial polymer mass remained as residue. The reduced catalytic cracking capacity of PtHMCM-41 arising from its lower acidity resulted in the dominance of large paraffins ($>C_8$) in the hydrocracking product slate (Fig. 8). Similar to the PtHY catalyst, the PtHMCM-41 volatile paraffin evolution profile in hydrogen was narrower and shifted to a higher temperature ($\sim$ 20°C) compared to the helium profile. Although paraffin evolution effective activation energies in helium could not be computed, the shift to higher temperatures suggests increased activation energy for hydrocracking processes.

Hydrocracking effective activation energy plots for the three catalysts used in this study all exhibit a decrease with increasing temperature above 240°C. The magnitude of the drop in activation energy follows the trend: PtHMCM-41 > PtHY > PtHZSM-5. It has been previously reported that the strength of olefin adsorption on catalyst surfaces determines the kinetics of platinum catalyzed hydrogenation.[34] The strength of olefin adsorption would be expected to

decrease with an increase in catalyst temperature, which would explain the observed decrease in activation energy for each catalyst. The activation energy decrease was much greater for PtHMCM-41 than the other catalysts. The attraction of olefins to PtHMCM-41 catalyst surfaces would be expected to be much less than the other catalysts because of its relatively low acidity. Apparently, interactions between olefins and PtHMCM-41 catalyst surfaces diminish more rapidly with increased temperature than the other catalysts.

CONCLUSION

Because PE/catalyst samples contained much more catalyst than polymer, effects from deactivation processes were minimal and results described here reflect innate catalyst activities. Hydrocracking reactions dominated when polyethylene was catalytically cracked in the presence of hydrogen. The length of volatile paraffins was found to depend on the catalyst pore size and acidity and followed the trend: PtHMCM-41 > PtHY > PtHZSM-5. Volatile product slate and effective activation energy trends cannot be explained by a single catalyst characteristic. Instead, the combined influence of acidity, pore size, and preferred cracking mechanism(s) for each volatile product must be considered.

References

1. Municipal Solid Waste in the United States: 2000 Facts and Figures; EPA530-R-02-001; U.S. Environmental Protection Agency, Office of Solid Waste and Emergency Response (5305W), U.S. Government Printing Office: Washington, DC, June 2002.
2. The Resource Conservation Challenge—Making the Connection with Solid Waste Facts and Figures; EPA; U.S. Government Printing Office: Washington, DC, 2001.
3. U.S. Plastics Economic Impact Overview; The Society of the Plastics Industry, Inc.: Washington, DC, 2002.
4. Ochoa, R.; Van Woert, H.; Lee, W. H.; Subramanian, R.; Kugler, E.; Eklund, P. C. Fuel Proc Tech 1996, 49, 119.
5. Aguado, J.; Serrano, D. P.; Romero, M. D.; Escola, J. M. Chem Commun 1996, 725.
6. Aguado, J.; Sotelo, J. L.; Serrano, D. P.; Calles, J. A.; Escola, J. M. Energy Fuels 1997, 11, 1225.
7. Sakata, Y.; Uddin, M. A.; Muto, A.; Kanada, Y.; Koizumi, K.; Murata, K. J Anal Appl Pyrolysis 1997, 43, 15.
8. Sakata, Y. in Recycling of Polymers; Kahovec, J., Ed.; Wiley-VCH: Weinheim, Germany, 1998; pp. 7–18.
9. Sharratt, P. N.; Lin, Y.-H.; Garforth, A. A; Dwyer, J. Ind Eng Chem Res 1997, 36, 5118.
10. Garforth, A. A.; Lin, Y.-H.; Sharratt, P. N; Dwyer, J. Appl Catal, A 1998, 169, 331.
11. Dufaud, V.; Basset, J. M. Angew Chem Int Ed 1998, 37, 806.
12. Ding, W.; Liang, J.; Anderson, L. L. Energy Fuel 1997, 11, 1219.
13. Walendziewski, J.; Steininger, M. Catal Today 2002, 65, 323.
14. Walendziewski, J. Fuel 2002, 81, 473.
15. Garforth, A.; Fiddy, S.; Lin, Y.-H.; Ghanbari-Siakhali, A.; Sharratt, P. N; Dwyer, J. Thermochim Acta 1997, 294, 65.
16. Fernandes, Jr., V. J.; Araujo, A. S.; Fernandes, G. J. T. J Thermal Anal 1997, 49, 355.
17. Fernandes, Jr., V. J.; Araujo, A. S.; Fernandes, G. J. T. J Thermal Anal Calorim 1999, 56, 275.
18. Lin, Y.-H.; Sharratt, P. N.; Garforth, A. A.; Dwyer, J. Thermochim Acta 1997, 294, 45.
19. Hesse, N. D.; Lin, R.; Bonnet, E.; Cooper, III, J.; White, R. L. J Appl Polym Sci 2001, 82, 3118.
20. Bonnet, E.; White, R. L. Instr Sci Tech 2001, 29, 317.
21. Bonnet, E.; White, R. L. Thermochim Acta 1998, 311, 81.
22. Kresge, C. T.; Leonowicz, M. E.; Roth, W. J.; Vartuli, J. C.; Beck, J. S. Nature 1992, 359, 710.
23. Schmidt, R.; Akporiaye, D.; Stocker, M.; Ellstad, O. H. J Chem Soc Chem Commun 1994 1943.
24. Beck, J. S.; Vartuli, J. C.; Roth, W. J.; Leonowicz, M. E.; Kresge, C. T.; Schmitt, K. D.; Chu, C. T. W.; Olson, D. H.; Sheppard, E. W.; McCullen, S. B.; Higgins, J. B.; Schlenker, J. L. J Am Chem Soc 1992, 114, 10834.
25. Jacobs, G.; Ghadiali, F.; Pisanu, A.; Borgna, A.; Alvarez, W. A.; Resasco, D. E. Appl Catal, A 1999, 188, 79.
26. Weisz, P. B.; Swegler, E. W. Science 1957, 126, 31.
27. Paal, Z.; Menon, P. G. Catal Rev Sci Eng 1983, 25, 229.
28. Weisz, P. B. Adv Catal 1962, 13, 137.
29. Maegaard, S.; M.Sc. dissertation, University of Manchester Institute of Science and Technology, 1997.
30. Lin, Y. H.; Hwu, W. H.; Ger, M. D.; Yeh, T. F.; Dwyer, J. Mol Catal, A 2001, 171, 143.
31. Wojciechowski, B. W. Catal Rev Sci Eng 1998, 40, 209.
32. Ribeiro, F.; Marcilly, C.; Guisnet, M. J Catal 1982, 78, 267.
33. Perrotin, L.; Finiels, A.; Fajula, F.; Cholley, T. Stud Surf Sci Catal 2001, 135, 3838.
34. Navalikhina, M. D.; Krylov, O. V. Russ Chem Rev 1998, 67, 587.